The Pierre Auger Observatory – a new stage in the study of the ultra-high energy cosmic rays

Serguei Vorobiov[a]*, for the Pierre Auger Collaboration[b]†
[a] *Laboratory for astroparticle physics, University of Nova Gorica*
Vipavska 13, POB 301, SI-5001 Nova Gorica, Slovenia
[b] *Pierre Auger Observatory*
Av. San Martín Norte 304, (5613) Malargüe, Mendoza, Argentina

Abstract

This paper presents the highlights from the recent measurements of the energy spectrum, mass composition, and arrival directions of the ultra-high energy ($\geq 10^{17}$ eV) cosmic rays (UHECR) by the Pierre Auger Observatory. The Auger hybrid detector combines fluorescence observations of the longitudinal profiles of extended air showers, initiated by these extremely energetic particles, with measures of the shower secondaries at the ground level by its large array of Cherenkov water tanks. The complementariness of the two techniques provides important cross-checks at the energies unreachable with accelerator experiments. The Pierre Auger experiment has observed a strong steepening of the cosmic ray flux above 4×10^{19} eV. A significant anisotropy in the arrival directions of cosmic rays has been established for events above $\simeq 6 \times 10^{19}$ eV. These events correlate over angular scales of less than 6° with the directions towards nearby ($D < 100$ Mpc) active galactic nuclei. Both observations are consistent with the standard scenarios of the UHECR production in the extra-galactic astrophysical acceleration sites. The derived stringent upper limits on the photon and neutrino contents in the UHECR are additional important arguments in support of these scenarios. The measurements of the variation of the depth of shower maximum with energy, interpreted with the current hadronic interaction models, favour the mixed cosmic ray composition at energies above 4×10^{17} eV. We describe the plans and prospects for the future, that will further help to solve the 50 years old UHECR puzzle.

Introduction

After nearly a century of investigations, cosmic rays (CR) still represent a scientific challenge and offer fundamental questions about their origin and nature. The CR energy spectrum remarkably shows only little deviation from a constant power law $J(E) \propto E^{-2.7}$ across the large energy range from 10^9 eV to 10^{20} eV. The main paradigm for explanation of this non-thermal spectrum is the diffusive acceleration of charged particles in the vicinity of astrophysical shocks. The small variations of the spectral index are signs of possible changes in the CR acceleration and/or propagation regimes. The significant increase in the slope of the CR spectrum to $E^{-3.0}$ occurs at the so-called knee near 5×10^{15} eV, and is presently attributed to a maximum energy expected in the diffusive shock acceleration in Galactic supernova remnants (SNR). At much higher energies, corresponding to the "ankle" observed at $\sim 4 \times 10^{18}$ eV, the spectrum becomes again $E^{-2.7}$. The integral cosmic ray flux above the ankle is only about 1 particle per km^2 steradian year, which implies the need for huge detectors to collect substantial statistics.

Supernova remnants are thought to be prime candidates for the acceleration of galactic cosmic rays up to energies of several 10^{17} eV. At these ultra-high (UHE, E $\geq 10^{17}$ eV) energies,

*e-mail: sergey.vorobyev@p-ng.si
†e-mail: info@auger.org.ar

only a few astrophysical acceleration sites unify the conditions (sufficiently large size, strong magnetic fields) allowing to efficiently produce the cosmic rays, a list of candidates being limited to objects like active galactic nuclei, gamma-ray bursts or galaxy clusters. Coincidentally, the cosmic rays above $\geq 10^{17}$ eV are able to arrive on Earth from regions external to the Local Group of galaxies (D $\sim$ 3 Mpc). Above $\geq 10^{19}$ eV, the bulk of the UHECR is believed to be extragalactic, which is comforted by the non-observation of anisotropies connected with the Galactic plane.

If this standard acceleration scenario with the nuclei arriving from sources at cosmological distances holds, it is expected that the cosmic ray flux should undergo a strong suppression (so-called GZK cut-off [1]) at energies above $\sim 5 \times 10^{19}$ eV. This spectral break corresponds to the effective threshold of pion production in the interaction of the UHECR protons with the CMB radiation. At similar energies, nuclei photo-dissociate on the CMB. As a consequence, the horizon of the UHECR sources in the standard scenarios is restricted to our local "neighbourhood" ($\simeq$ 50 Mpc). Above the GZK cut-off, the deflections of cosmic rays in the galactic and intergalactic magnetic fields are minimal, and individual CR sources should be observed.

Alternatively, more exotic UHECR scenarios have been proposed. In some of these scenarios, cosmic rays are produced in interactions or decays of the primordial Universe relics such as topological defects or super-heavy dark matter. Contrary to the astrophysical acceleration scenarios, these "top-down" UHECR production models predict a substantial fraction of primary photons and neutrinos.

To distinguish between different UHECR scenarios, it is crucial to measure precisely the cosmic ray arrival direction distribution, primary mass composition, and energy spectrum. Since the UHECR fluxes are small, these highest energy particles are only detectable in an indirect way, through the extensive air showers (EAS) they create in the atmosphere. Above the energies around 10^{14} eV/nucleon, the technique of sampling the shower particles, predominantly electrons, gammas, and muons, by detectors on the ground becomes efficient. Lateral distributions of EAS particles, measured by surface detector arrays, reflect the particle densities in the tail of the shower far away from the shower axis, and serve to estimate the primary energy and mass. However, at the highest energies such estimates depend strongly on assumptions about the hadronic interactions, which are extrapolated to energies exceeding by far those accessible at man-made accelerators and in regions of phase space not covered in collider experiments. The advantages of surface detector arrays include stable operation with 100% percent duty cycle, and a relatively straightforward determination of the aperture.

In the UHE regime, where the Auger experiment operates, the air fluorescence technique allows estimation of the primary CR energy. As fluorescence light is produced proportional to the energy deposited in the atmosphere, this technique provides a calorimetric energy measurement that is fairly independent of the details of the shower development, and thus of our understanding of the individual hadronic interactions. Unfortunately, the fluorescence technique can only be used in dark, clear nights, which reduces its duty cycle to about 10%. Another drawback of this technique is that the aperture of a fluorescence detector grows with shower energy, and its determination for all operating conditions is nontrivial.

During the long period before the advent of the Pierre Auger Observatory, the world largest cosmic ray data set above 10^{19} eV has been collected by two experiments, each exploiting only one of these methods, either the detection of shower particles on the ground (AGASA surface array), or the fluorescence technique (HiRes). Consequently, the results of AGASA and HiRes were affected by different systematics. In addition, because of the small available statistics, the key issue of the presence of the GZK cut-off in the UHECR energy spectrum remained unclear. To improve this situation, the Auger Observatory was conceived in the 1990s [2] as a hybrid detector, combining the two detection techniques and covering an area 30 times larger than that of the AGASA array.

The Pierre Auger Observatory

The Pierre Auger Observatory for the ultra-high energy cosmic ray studies has been designed and built by an international collaboration of more than 350 scientists representing $\sim$ 100 institutions from 17 countries. The Observatory site in the province of Mendoza, Argentina will be completed in the year 2008. The Auger Surface Detector (SD) consists of 1600 water Cherenkov detectors, deployed over 3000 km^2 on a hexagonal grid with 1500 m spacing. The SD array is overlooked by the Auger Fluorescence Detector (FD), which comprises 24 fluorescence telescopes, arranged in four sites at the perimeter of the SD area. This hybrid design allows the simultaneous detection of the same cosmic ray events by two complementary techniques, which provides important cross-checks and measurement redundancy. The Auger Detector layout and the status of deployment as of June 2008 is shown on the Fig.1. The properties and performance of the hybrid instrument can be found in [3, 4].

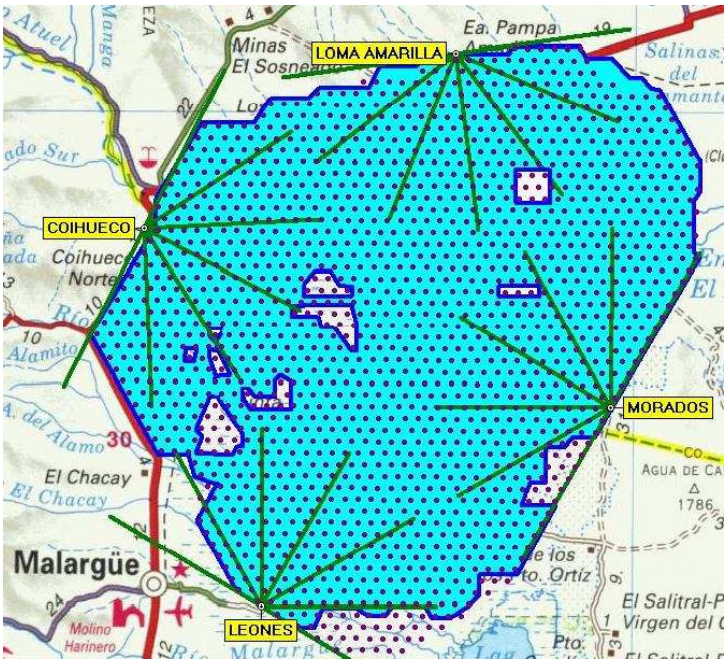

Figure 1: Deployment status of the Pierre Auger Observatory, as of June 2008. The points on the hexagonal grid show the positions of the water Cherenkov detectors. The shaded area marks the surface detectors in operation. The four named fluorescence detectors with six individual telescopes at the perimeter of the surface array are all operational. The central campus is located in the town of Malargüe.

Each Surface Detector station consists of a polyethylene tank, 1.55 m high and 3.6 m diameter, enclosing a liner filled with 12 tons of purified water. Three 9 inch diameter photomultiplier tubes (PMTs), located symmetrically at a distance of 1.2 m from the center of the tank, look downward through windows in the liner and collect the Cherenkov light from the passage of showers particles in the water. The PMT signals are digitized at 40 MHz sampling frequency, which provides a temporal resolution of 8 ns. The electronics package also includes GPS receiver and a radio communication system. Each tank is equipped with a 10 Watt solar power system and operates in an autonomous manner. A robust, automatic calibration procedure of the SD detectors [5] uses the measurement of the average charge, collected by a PMT from the Cherenkov light produced by relativistic muons passing vertically through the center of a tank. Subsequent measures of the signal are given in such vertical equivalent muon (VEM) units. The SD calibration procedure is carried out continuously, and enables to determine the signals recorded from extensive air showers with 3% accuracy. It also allows to achieve stable

and uniform triggering conditions through the whole SD array.

A hierarchical trigger sequence is applied to ensure the rejection of accidental triggers in order to retain the physical events. Then the tank signal timing information and the integrated charge values are used for reconstruction of shower geometry (arrival direction and core position). The measured signals as a function of distance from the shower axis are fitted for individual events to obtain the water Cherenkov signal at a distance of 1000 m, S(1000), which serves as an estimator of the size of each event. Simulations show that both for proton- and iron-induced showers the S(1000) parameter is almost proportional to primary energy. Also, at these distances from the axis the fluctuations of lateral distribution of particle density are minimal for studied energies and adopted array geometry, for zenith angles $\theta < 60^\circ$. The overall uncertainty in S(1000) at energies around 10^{19} eV is about 10%, and improves with energy [6]. For S(1000) < 40 VEM (which corresponds to energies lower than $\sim 6 \times 10^{18}$ eV), the main contribution to the uncertainty is due to the finite dimension of the detectors and the small counting statistics. At higher energies, the major contribution to the uncertainty in S(1000) arises from the fluctuations in the shower development and the consequent lack of knowledge of the true lateral particle distribution shape for a particular event.

The angular resolution of the surface detector was determined from the shower front arrival times, on an event by event basis, and checked using the data from the pairs of SD stations located ~ 11 m apart (see [6] and the references therein). The resolution was found to be better than 2° for 3-fold events (events with 3 stations participating in the event, which corresponds to energies $E < 4 \times 10^{18}$ eV), better than 1.2° for 4-fold and 5-fold events ($3 \times 10^{18} < E < 10^{19}$ eV) and better than 0.9° for higher multiplicity events ($E > 10^{19}$ eV).

The "quality" cuts, which are used in most analyses, select among the physical events those with the highest signal recorded in a tank surrounded by six operating ones, and with the reconstructed core within a triangle of working stations. Also, the events with arrival zenith angles $\theta < 60^\circ$ are considered. These selection criteria guarantee that showers are sufficiently well contained within the SD array to allow a robust measurement of S(1000) and the shower axis. The quality cuts result in a 100% combined trigger and reconstruction efficiency above 3×10^{18} eV [7]. At higher energies, the effective area of the SD array at any time is calculated from the number of active hexagons, which can be determined from the low-level triggers sent by each station every second (see [7] and the references therein).

The Auger Fluorescence Detectors measure the faint ultra-violet light emitted as the shower traverses the atmosphere. Each of the 24 individual Schmidt design telescopes covers a 30° range in azimuth and $0^\circ \div 30^\circ$ range in elevation. A 11 m^2 segmented spherical mirror (radius of curvature 3.4 m) is focusing the light from the 2.2 m diameter diaphragm onto a camera of 20×22 PMTs, each with a field of view of 1.5° in diameter. The PMT signals are digitized at 100 MHz sampling rate. At the diafragm opening, there is a ring corrector lens to double the light collection efficiency and to reduce the aberrations, and a UV-transparent filter window, which also serves as a protection from dust.

The optical and electronics calibration of the FD system is known to 9.5%. The absolute end-to-end calibration is performed periodically through the year, using a uniformly illuminated drum positioned at the diafragm aperture. The NIST calibrated light source with known intensity and spectral and directional characteristics allows for measurements at five wavelengths. The relative calibration, made twice every night with pulsed LEDs and/or Xe flashers, keeps track of any changes between the drum calibrations.

The atmosphere is an integrated part of the FD operation, and the attenuation of the fluorescence light due to Rayleigh and aerosol scattering along its path toward the telescope have to be carefully monitored. Each FD site is equipped with a single wavelength LIDAR. Regular balloon launches are performed to measure vertical profiles of the air temperature and pressure. The atmospheric monitoring system also includes one Raman LIDAR, a meteo station per FD

site, a remote-controlled centrally positioned YAG laser, and dedicated aerosol monitors and cloud cameras. The systematic uncertainties in atmospheric attenuation contribute approximately 4% to the systematic uncertainty for shower energy estimate. For the energy deposited in the atmosphere by shower particles the data from [8] are currently being applied, with the systematic uncertainty in the absolute fluorescence yield of 14%. The measurements from [9] are used for the wavelength and pressure dependence of the fluorescence spectrum. Uncertainty related to pressure, temperature and humidity effects amounts to 7%.

The image of a shower developing in the field of view of a telescope represents a track of triggered PMTs, which enables to reconstruct a shower-detector plane (SDP) with a high precision ($\simeq 0.3^\circ$). The pixel timing information is used to determine the shower direction. When, in addition to an FD telescope, one or more SD tanks participate in the event (hybrid detection), the SD timing information improves considerably the shower geometry reconstruction. Compared to the case of mono FD events, the accuracy of angular reconstruction and of the determination of the core position of the showers are both improved about a factor of 10.

In the algorithm used to reconstruct the longitudinal profile of a shower, care must be taken to collect the fluorescence light without inclusion of the night-sky background, and to properly account for a contribution of direct and scattered Cherenkov light. The reconstructed profile of the energy deposit, fitted with a Gaisser-Hillas function [10], provides a measurement of the shower energy, and of X_{max}, the depth of the shower maximum. Systematic uncertainties in the reconstruction method contribute 10% to the total uncertainty in the measured energy. A final small correction ($\simeq 10\% \pm 4\%$ at the Auger energies) takes into account the "missing" energy due to muons and neutrinos.

The quality cuts applied to the hybrid events selected for the data analysis are described in [11]. The hybrid method provides a nearly calorimetric, model-independent energy measurement with a statistical resolution of 8%. The corresponding resolution in X_{max} is 20 g/cm^2. The quoted systematic uncertainties in the energy scale by the hybrid method (see [4] and the references therein) add up to 22%, the largest contributions being due to the uncertainties in the absolute fluorescence yield (14%) and the absolute FD calibration (10%).

The results reported here are essentially based on the analysis of the data collected at the Pierre Auger Observatory between 1 January 2004 and 31 August 2007. During this time, the SD array grew from 154 to 1388 tanks, and the number of FD telescopes increased from 6 to 24. The integrated exposure over this period is four times greater than that of AGASA, similar to the monocular HiRes exposure, and is equivalent to roughly 1 year of operation of the full Auger array. Above 10^{18} eV, the Auger Observatory has recorded more events than all previous experiments together. The expected future annual increment of the exposure is 7000 km^2 sr yr.

The UHECR energy spectrum

The hybrid nature of the Auger detector allowed a measurement of the energy spectrum to be made with high statistics, and with small dependence on assumptions about hadronic interaction models or the primary mass composition. We use the constant integral intensity cut method, which exploits the nearly isotropy of cosmic rays, to rescale S(1000) value from different zenith angles θ. The choice of the threshold S(1000) value is not critical, since the shape of the attenuation curve giving intensity I(>S(1000)) in equal solid angle bins of $\cos^2\theta$ is within the statistics nearly the same in the large range of S(1000) [12]. We normalize S(1000) for each event to the signal it would have produced at a zenith angle of 38°, which is the median value for zenith angles of interest. We establish the relation between that quantity called S_{38°, and the calorimetric FD energy measurement for currently 661 selected high-quality hybrid events. A clear correlation between the two energy estimators can be seen on the left plot in Fig. 2. A power law fit to the data is performed, yielding $E_{\rm FD} = 1.49 \times 10^{17}{\rm eV} \times S_{38^\circ}^{1.08}$, which shows

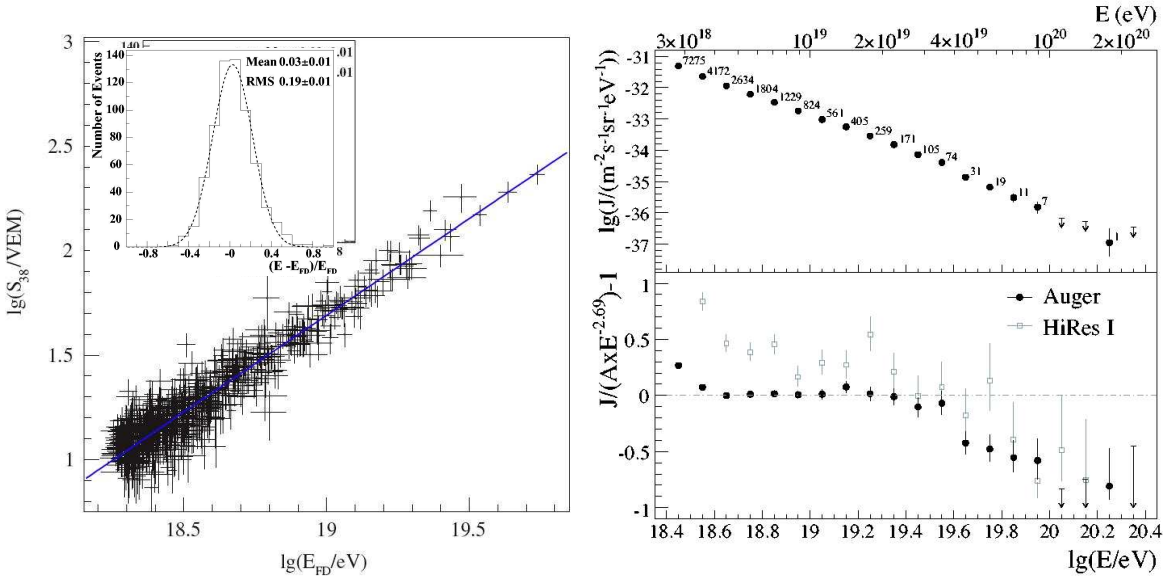

Figure 2: The energy calibration by the hybrid method and the resulting Auger UHECR energy spectrum [13]:
(left) Correlation between SD energy parameter S_{38° and FD energy for the 661 hybrid events used in the fit. The full line is the best fit to the data; the fractional differences between the two energy estimators are shown in the inset.
(right) Upper panel: Differential flux as a function of energy, with statistical uncertainty. The number of events in each bin is also shown. Lower panel: Fractional differences between Auger and HiRes I data compared to a spectrum with an index of 2.69.

that S_{38° grows approximately linearly with energy. The energy resolution, estimated from the r.m.s. deviation of the distribution, is 19%, which is in good agreement with the quadratic sum of the SD and FD energy statistical uncertainties of 18%.

The energy spectrum based on 20,000 SD events is shown on the right plot in Fig. 2. The systematic uncertainty in the absolute energy scale set by the FD is 22%, as described in the previous section. The spectrum between 4×10^{18} eV and 4×10^{19} eV is well approximated by a power law with the slope $-2.69 \pm 0.02(\mathrm{stat}) \pm 0.06(\mathrm{syst})$, where the systematic uncertainty comes from the calibration curve. If this slope is extrapolated to higher energies, the expected number of events above 4×10^{19} eV and 10^{20} eV is 167 ± 3 and 35 ± 1, while 69 events and 1 event are observed. The Auger data therefore clearly show that the slope of the spectrum increases above 4×10^{19} eV, with the significance of the steepening being more than 6 standard deviations. Above this energy, the spectral index is $-4.2 \pm 0.4(\mathrm{stat}) \pm 0.06(\mathrm{syst})$. On Fig. 2, fractional differences relative to a spectrum $J(E) \propto E^{-2.69}$ are also shown, together with the data from the HiRes I experiment [14]. The AGASA data are not shown, since they are currently under revision [15].

The Auger UHECR energy spectrum measurements have been extended to the zenith angle range between 60° and 80°. A dedicated reconstruction procedure has been implemented [16] for such inclined events, dominated by muons. The shower axis and the total number of muons are reconstructed using simulation-based maps of the muon ground density. The hybrid Auger events are used in the similar way as above to establish the relationship between the muon number and the energy measured by FD. A total of 734 events above 6.3×10^{18} eV were used to build the spectrum [17]. The integrated exposure for this measurement is 1510 km^2 sr yr, which corresponds to 29% of the respective exposure for events below 60°.

The Auger spectrum has also been extended to lower energies down to 10^{18} eV, using hybrid events [18]. The three energy spectrum measurements (using SD vertical, SD inclined

and hybrid events) are consistent where they overlap. The astrophysical implications of the measured UHECR energy spectrum that features flux suppression above 4×10^{19} eV and the steepening below the ankle at $\sim 4 \times 10^{18}$ eV (see Fig. 2) are discussed in [19].

Mass composition studies using X_{max}

The hybrid technique allows for precise measurement of the depth of shower maximum as a function of energy. Heavy nuclei are expected to reach the maximum development at smaller average depths than protons and to produce smaller shower-to-shower fluctuations. The cosmic ray mass composition can therefore be studied by comparing the observed average X_{max} with predictions from air shower simulations for different nuclei. The change of average X_{max} with energy is used to probe the changes in primary composition. The Auger result [11] based on 4329 hybrid events across two decades of energy is shown on Fig. 3. The left plot compares the Auger measurements with predictions for proton and iron primaries made using three models of hadronic interactions. If the interaction models are correct, the Auger data favour mixed composition for all energies above 4×10^{17} eV. However, there are indications that the hadronic models may need modification [20]. There is a general agreement with the results from previous experiments, as it can be seen from the right plot on the same figure. At the same time, the Auger measurement is more precise and covers larger energy range. The apparent change from lighter to heavier mass composition above 2×10^{18} eV is currently examined by studying the fluctuations in X_{max} at a given energy.

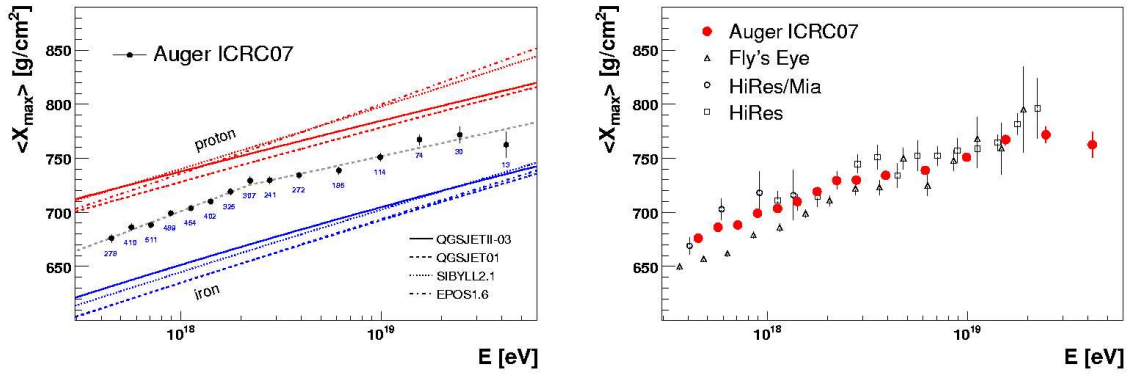

Figure 3: Auger measurements [11] of the average depth $\langle X_{max} \rangle$ of shower maximum as a function of energy. *(left)* $\langle X_{max} \rangle$ compared to predictions from hadronic interaction models for primary protons and iron nuclei. The dashed line shows results of a fit with two constant elongation rates and a break-point. The number of events in each bin is indicated below the data points. *(right)* $\langle X_{max} \rangle$ compared to forerunner experiments.

The photon and neutrino limits

The presence of photons and neutrinos in the UHECR is guaranteed due to the interactions of cosmic ray nuclei with background radiation fields via the production of neutral and charged pions $\pi^0, \pi^\pm$ and their subsequent decays. A discovery of these "GZK" photons and neutrinos would provide a unique opportunity to trace back their production sites, and to test fundamental particle physics at energies well beyond current or planned accelerators.

Showers induced by the UHE photons develop deeper in the atmosphere than those initiated by the primary nuclei, and contain fewer muons. The first Auger limit on photon contents in the UHECR had been derived exploiting the X_{max} measurement in hybrid events [21]. A more strin-

gent limit has now been obtained [22] using the large SD event statistics. Two photon-sensitive SD observables have been combined in the analysis: the risetime of the recorded shower signal and the radius of curvature of the shower front. Since photons are less efficient in triggering the Auger Surface Detector, the analysis has been limited to energies higher than 10^{19} eV, and to zenith angles θ between 30° and 60°. The photon energy scale has been estimated with a help of a custom reconstruction that accounted for the universality of the development of the electromagnetic component of showers for depths exceeding X_{max}. A search for photon candidates in the Auger SD data has been performed, and no candidate has been found. This allowed us to obtain upper limits on photon flux and fraction above 10, 20, and 40 EeV (1 EeV $\equiv 10^{18}$ eV) at 95% confidence level (the respective limits on the photon fraction are 2.0%, 5.1%, and 31%; the corresponding limits on the photon flux are (in units of km^{-2} sr^{-1} yr^{-1}) $3.8 \times 10^{-3}, 2.5 \times 10^{-3}$, and 2.2×10^{-3}). The resulting Auger upper limits (see the left plot on Fig. 4) represent significant improvement upon the results from the previous experiments. They strongly constrain exotic models of UHECR production. With the accumulation of Auger data in the incoming years, the level expected for GZK photons may be reached.

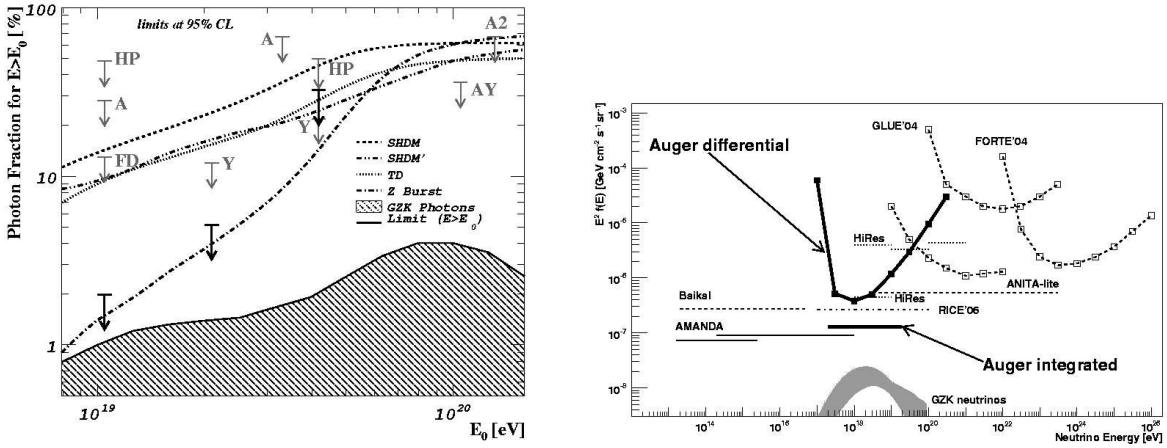

Figure 4: Limits on UHE photon and neutrino contents.
(left) The upper limits on the fraction of photons in the integral cosmic ray flux derived from Auger SD events (black arrows) along with the previous experimental limits (HP: Haverah Park; A, A1, A2: AGASA; AY: AGASA-Yakutsk; Y: Yakutsk; FD: Auger hybrid limit). Also shown are predictions from top-down models and for the GZK photon fraction. See [22] and the references therein.
(right) Limits at 90% C.L. for a diffuse flux of ν_τ from the Pierre Auger Observatory. Limits from other experiments are converted to a single flavour assuming a 1:1:1 ratio of the 3 neutrino flavours and scaled to 90% C.L. where needed. The shaded curve shows a typical range of expected fluxes of GZK neutrinos, although predictions almost 1 order of magnitude lower and higher exist. The references can be found in [25], where the figure is taken from.

A large air mass above the Auger SD array represents an important target for detection of showers induced by UHE neutrinos. Such showers can be identified if they develop deep in the atmosphere under large zenith angles, by the presence of a significant electromagnetic shower component. Two types of neutrino events can be detected by the SD array: down-going showers produced by a flux of neutrinos of all flavours [23], and upcoming showers initiated by the decay of τs emerging from the Earth after the propagation of a ν_τ flux [24]. Identification criteria have been developed to find EAS due to the UHE Earth-skimming neutrinos. No candidates have been found in the data collected between 1 January 2004 and 31 August 2007. Assuming an

E_ν^{-2} differential energy spectrum, we derive a 90% upper limit on the diffuse tau neutrino flux as $E_\nu^2 dN_{\nu_\tau}/dE_\nu < 1.3 \times 10^{-7}$ GeV cm^{-2} s^{-1} sr^{-1} in the energy range 2×10^{17} eV $< E_\nu < 2 \times 10^{19}$ eV. Our result [25], which is at present the most sensitive bound on neutrinos in the EeV energy range, is shown on Fig. 4.

Results on the UHECR anisotropies

The search for anisotropies in the arrival directions of cosmic rays has been a long-standing goal. If the observed suppression of the UHECR energy spectrum is due to the cosmic ray interactions with the CMB, the CR arrival directions at the energies above the suppression are expected to correlate with the nearby matter distribution, which is quite inhomogeneous. Observation of such correlations can constitute a first step towards doing the cosmic ray astronomy, provided that cosmic ray deflections in the intervening galactic and extragalactic magnetic fields are small enough, so that the CR arrival directions point back to their origin.

To test for possible correlations with extragalactic objects, the Pierre Auger Collaboration analysed [26, 27] the arrival directions of the events above 4×10^{19} eV, to search for coincidences with the positions of the nearby ($D < 100$ Mpc) active galactic nuclei (AGN) listed in the Véron-Cetty and Véron catalogue [28]. A scan over the maximum angular separation ψ between the events and the AGNs, the maximum considered AGN redshift $z_{\rm max}$, and the lower threshold energy $E_{\rm th}$ for cosmic ray events was performed to search for the most significant correlation. The range of the scanned parameter values has been chosen large enough, given the unknown intervening magnetic fields and cosmic ray mass composition (which would affect the amplitude of deflections, and also the GZK horizon distance) as well as the systematic uncertainties in energy determination.

A deep minimum in the probability P of observing a similar or larger number of correlations arising from simulated isotropic data sets was observed for $\psi = 3.2^\circ$, $z_{max} = 0.017$ (or maximum AGN distance of 71 Mpc) and $E_{th} = 57$ EeV (which corresponds to the 27 highest energy events). Under these parameters, only $\sim 10^{-5}$ of isotropic simulations have a deeper minimum. A correlation was first found in the data taken before the end of May 2006, for very similar parameter values. A test with this set of parameters, fixed *a priori*, has been applied to the subsequent data collected up to the end of August 2007, and the anisotropy has been confirmed using this independent data set at more than 99% confidence level.

The map of the arrival directions and of the AGN positions is shown on Fig. 5. Out of the 27 most energetic events, 20 are at less than 3.2° from an AGN closer than 71 Mpc, while only 5.6 events were expected on average if the CR flux were isotropic. A remarkable alignment of several events with the supergalactic plane is observed. Also, two events fall within 3.2° from Centaurus A, one of the closest active galaxies. It is worth to note that the energy maximizing the correlation with AGNs coincides with the one that maximizes the autocorrelation of the events [29], and also with the energy for which the cosmic ray flux decreases to 50% of the power law extrapolation (see Fig. 2).

The observed correlation suggests that the highest energy cosmic rays originate from nearby extragalactic sources, either AGN or other objects with a similar spatial distribution. This result is consistent with the hypothesis that the measured steepening of the spectrum above 40 EeV is due to the GZK effect, rather than to a maximum energy attainable in cosmic ray accelerators. The larger statistics and further investigations will help to unambiguously identify the UHECR sources.

At lower energies, the Pierre Auger Collaboration has performed search for extended and point-like sources in the Galactic Center region, and no significant excess has been found in the Auger data [30]. Also, searches for large-scale anisotropies have been performed by looking for patterns in the right ascension modulation of the cosmic ray distribution [31]. No anisotropy of

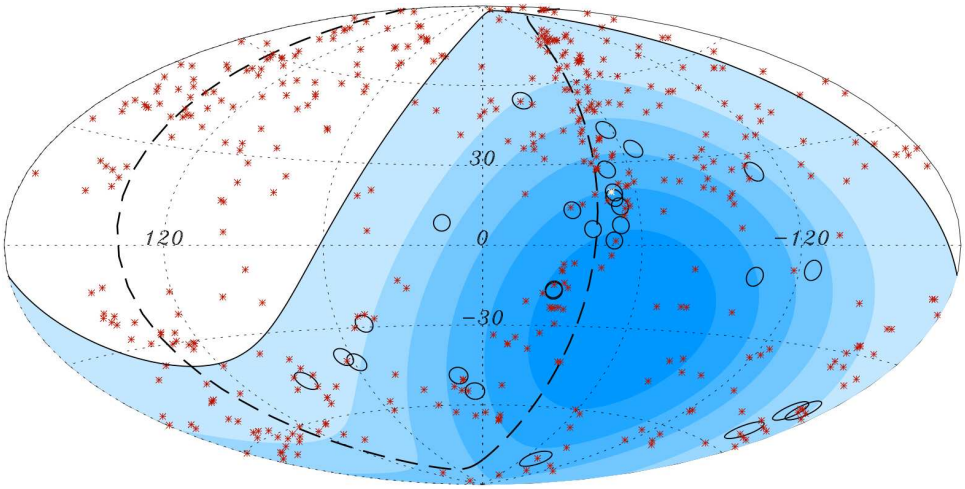

Figure 5: Map in galactic coordinates with circles of 3.2° radius centered on the arrival directions of the 27 Auger events with energy $E > 57$ EeV (taken from [26, 27]). The positions of the 442 AGN from the 12^{th} edition of the Véron-Cetty and Véron catalogue with redshifts $z \leq 0.017$ ($D < 71$ Mpc) are shown with red stars (one of the closest objects, Cen A, is shown in white). Shading within the solid line (the Auger field of view for $\theta < 60°$) indicates regions of equal exposure. The dashed line denotes the supergalactic plane.

this kind has been found, and an upper limit on the first harmonic modulation of 1.4% in the energy range $1 < \mathrm{E} < 3$ EeV was set.

Conclusions and future prospects

The recent Pierre Auger Observatory measurements of the UHECR energy spectrum, arrival directions and mass composition, albeit taken during the detector construction phase, have already significantly contributed to the progress in the field. The obtained results have demonstrated the power of the Auger hybrid design. The Southern Auger Observatory is now almost complete (the Surface Detector assembly and deployment activities have been essentially completed in August 2008). The Auger South will provide the good quality experimental data for at least ten years.

Since the elaboration of the Auger Project design report [2] in the 1990s, it was proposed to construct two similar instruments in both hemispheres, in order to cover the whole sky. In 2005, a site in Colorado, USA, has been chosen to host the Northern Auger Observatory. The Auger North will focus on the highest energy cosmic rays, with the aim to provide higher statistics at energies above the observed cosmic ray flux suppression. This will facilitate identification of individual nearby UHECR sources against the isotropic event background from the more distant objects, and thus will establish the long-sought charged particle astronomy.

To facilitate the data integration from both Observatories, Auger North will be built using the same basic elements as in the Southern Observatory: water Cherenkov detectors, fluorescence telescopes, and an associated infrastructure for communications and calibration. The performed research and development work has led to the design [32] of an array of $4,000$ surface detectors, covering the area of $8,000$ square miles, or $20,740\,\mathrm{km}^2$, i.e. ~ 7 times the Southern array. From 40 to 50 fluorescence telescopes will be needed for the almost full hybrid coverage of this large area. The envisaged layout of surface detectors (positioned with the spacing of $\sim 2.3\,\mathrm{km}$ on a square grid) will allow the array to be fully efficient for hadronic showers above 3×10^{19} eV. The proposal for Auger North is currently being finalized.

While it is clear that the highest energy cosmic rays arrive from extragalactic sources, it is currently not known at which energy the extragalactic CR flux becomes dominant. This question is central to the understanding of the nature of accelerators and their injection spectrum, as well as of the CR propagation in large-scale cosmic magnetic fields. Competing scenarios could be distinguished by better determination of CR mass composition and energy spectrum in the energy range between about 10^{17} eV and 3×10^{18} eV, where the transition between Galactic and extragalactic cosmic rays is expected [33].

Two hybrid "low" energy extensions of the Southern Auger Observatory (Auger Enhancements) will explore this energy range. New fluorescence detector, a system of three High Elevation Auger Telescopes (HEAT), is currently being installed near the Coihueco fluorescence site. The first telescope is expected to be operational in November 2008, and the last two will be operational in early 2009. HEAT will cover a range of elevation angles from 30° to 60°. The combined shower data of the Coihueco and the HEAT telescopes will lead to better resolutions for the determination of air shower energy and X_{max}, especially below $\sim 10^{18}$ eV [34].

To extend the hybrid technique down to $\sim 10^{17}$ eV, a denser array of water Cherenkov detectors of present design is currently being deployed on a $23.5\,\mathrm{km}^2$ area centered 6 km away from the fluorescence detector installations at Coihueco site. Each water Cherenkov detector will be accompanied by a $30\,\mathrm{m}^2$ muon scintillator counter buried alongside 3 m underground. The whole complex, baptized AMIGA (Auger Muons and Infill for the Ground Array) will consist of 85 pairs of water Cherenkov and muon detectors, placed on 433 and 750 m triangular grids. AMIGA surface detectors will complement the fluorescence measurements, and the muon detectors will be used to determine the mass composition in the range $10^{17} \div 5 \times 10^{18}$ eV [35].

Within the Auger Collaboration, there is also an active program to investigate the radio emission of extensive air showers in the $10 \div 100$ MHz band [36]. This method for shower studies, first introduced in the 1960s, has revived recently due to the new radio measurement techniques. The radio shower detection is exploitable with a 100% duty cycle, and provides additional information on the development of the electromagnetic shower component, which can be used to measure the primary CR energy, arrival direction, and mass in a way complementary to the SD and FD techniques. The tests of radio detection of showers with various antenna systems are currently being performed on the Southern Auger site. A recently obtained funding will allow the construction of a $20\,\mathrm{km}^2$ engineering array at the location of AMIGA infill. This engineering array will serve to the development of radio detection, with a goal to elaborate a design of a much larger array, that will cover an area of many thousand km^2.

Acknowledgements

I would like to thank the organizers of the 15^{th} International Seminar "QUARKS-2008", and of the accompanying 4^{th} International UHECR Workshop, for inviting me to present the results of the Pierre Auger Collaboration at both conferences. The support from the University of Nova Gorica is gratefully acknowledged.

References

[1] K. Greisen, Phys. Rev. Lett. **16**, no. 17 (1966) 748 ; G. T. Zatsepin and V. A. Kuz'min, Pis'ma Zh. Eksp. Teor. Fiz. **4**, no. 3 (1966) 114.

[2] The Pierre Auger Project Design Report, `http://www.auger.org/admin/DesignReport` .

[3] J. Abraham *et al.*, [Pierre Auger Collaboration], NIM **A523** (2004) 50.

[4] B. Dawson for the Pierre Auger Collaboration, Proc. 30$^{\text{th}}$ ICRC in Mérida (Yucatán, México, 3-11 July 2007), paper no. 976 ; the compilation of the Pierre Auger Collaboration activities and results presented at the 30$^{\text{th}}$ ICRC can be found at `http://www.auger.org/technical_info/icrc_2007.html` .

[5] X. Bertou et al., Nuclear Instruments and Methods A568 (2006) 839.

[6] M. Ave for the Pierre Auger Collaboration, Proc. 30$^{\text{th}}$ ICRC, paper no. 297.

[7] D. Allard for the Pierre Auger Collaboration, Proc. 29$^{\text{th}}$ ICRC, paper no. 134.

[8] M. Nagano et al., Astropart. Phys. 22 (2004) 235.

[9] M. Ave et al. (AIRFLY Collaboration), Astropart. Phys. 28 (2007) 41.

[10] T.K. Gaisser and A.M. Hillas, Proc. 15th ICRC, Vol. 8 (1977) p. 353.

[11] M. Unger for the Pierre Auger Collaboration, Proc. 30$^{\text{th}}$ ICRC, paper no. 594.

[12] M. Roth for the Pierre Auger Collaboration, Proc. 30$^{\text{th}}$ ICRC, paper no. 313.

[13] J. Abraham *et al.*, [Pierre Auger Collaboration], PRL 101 (2008) 061101.

[14] R.U. Abbasi et al., Phys. Rev. Lett. 100 (2008) 101101.

[15] M. Teshima, Roma Int. Conf. on Astroparticle Physics (RICAP), 2007.

[16] D. Newton for the Pierre Auger Collaboration, Proc. 30$^{\text{th}}$ ICRC, paper no. 308.

[17] P. Facal San Luis for the Pierre Auger Collaboration, Proc. 30$^{\text{th}}$ ICRC, paper no. 319.

[18] L. Perrone for the Pierre Auger Collaboration, Proc. 30$^{\text{th}}$ ICRC, paper no. 316.

[19] T. Yamamoto for the Pierre Auger Collaboration, Proc. 30$^{\text{th}}$ ICRC, paper no. 318.

[20] R. Engel for the Pierre Auger Collaboration, Proc. 30$^{\text{th}}$ ICRC, paper no. 605.

[21] J. Abraham *et al.*, [Pierre Auger Collaboration], Astroparticle Physics 27 (2007) 155-168.

[22] J. Abraham *et al.*, [Pierre Auger Collaboration], Astroparticle Physics 29 (2008) 243-256.

[23] E. Zas, New Journal of Physics 7 130 (2005); J. Alvarez-Muñiz for the Pierre Auger Collaboration, Proc. 30$^{\text{th}}$ ICRC, paper no. 607.

[24] D. Fargion, Astrophys. J. 570 (2002) 909 ; A. Letessier-Selvon, AIP Conf. Proc. 566 (2001); J. L. Feng et al., Phys. Rev. Lett. 88 (2002) 161102; P. Billoir, O. Blanch Bigas, et al. (Pierre Auger Collaboration), Nucl. Phys. B, Proc. Suppl. 168 (2007) 225.

[25] J. Abraham *et al.*, [Pierre Auger Collaboration], Phys. Rev. Lett. 100 (2008) 211101.

[26] J. Abraham *et al.*, [Pierre Auger Collaboration], Science, 318 (2007) 939-943.

[27] J. Abraham *et al.*, [Pierre Auger Collaboration], Astroparticle Physics 29 (2008) 188-204.

[28] M.-P. Véron, P. Véron, Astron. & Astrophys. **455** (2006) 773–777.

[29] S. Mollerach for the Pierre Auger Collaboration, Proc. 30$^{\text{th}}$ ICRC, paper no. 74.

[30] J. Abraham *et al.*, [Pierre Auger Collaboration], Astroparticle Physics 27 (2007) 244-253 ; E. Santos for the Pierre Auger Collaboration, Proc. 30$^{\text{th}}$ ICRC, paper no. 73.

[31] E. Armengaud for the Pierre Auger Collaboration, Proc. 30$^{\text{th}}$ ICRC, paper no. 76.

[32] D. Nitz for the Pierre Auger Collaboration, Proc. 30$^{\text{th}}$ ICRC, paper no. 180 ; J. Blümer for the Pierre Auger Collaboration, Proc. of the International Workshop on Advances in Cosmic Ray Science, Waseda University, Tokyo, Japan, 2008; [arXiv:astro-ph/0807.4871].

[33] G. Medina-Tanco for the Pierre Auger Collaboration, Proc. 30$^{\text{th}}$ ICRC, paper no. 991.

[34] H. Klages for the Pierre Auger Collaboration, Proc. 30$^{\text{th}}$ ICRC, paper no. 65.

[35] A. Etchegoyen for the Pierre Auger Collaboration, Proc. 30$^{\text{th}}$ ICRC, paper no. 1307.

[36] A.M. van den Berg for the Pierre Auger Collaboration, Proc. 30$^{\text{th}}$ ICRC, paper no. 176.